A&A 467, 371–374 (2007)
DOI: 10.1051/0004-6361:20065821

Astronomy & Astrophysics

Anomalous absorption in c-C_3H and c-C_3D radicals⋆ *(Research Note)*

S. Chandra[1,2], S. V. Shinde[2], W. H. Kegel[1], and E. Sedlmayr[1]

[1] Zentrum für Astronomie und Astrophysik, Technische Universität Berlin, Hardenbergstrasse 36, 10623 Berlin, Germany
e-mail: [kegel;sedlmayr]@astro.physik.tu-berlin.de
[2] School of Physical Sciences, S. R. T. M. University, Nanded 431 606, India
e-mail: suresh492000@yahoo.co.in

Received 14 June 2006 / Accepted 9 February 2007

ABSTRACT

Context. The c-C_3H radical was first detected in TMC-1 by Yamamoto et al. (1987, ApJ, 322, L55), who observed the $2_{12} \rightarrow 1_{11}$ transition at 91.5 GHz in emission. Mangum & Wootten (1990, A&A, 239, 319) observed the $1_{10} \rightarrow 1_{11}$ transition at 14.8 GHz in emission in 12 additional galactic objects.
Aims. The aim of this investigation is a quantitative estimate of relative line intensities under NLTE conditions.
Methods. For wide ranges of physical parameters, where these molecules may be found, we have solved a set of statistical equilibrium equations coupled with the equations of radiative transfer in an on-the-spot approximation. For c-C_3H, we accounted for 51 energy levels connected by 207 radiative transitions, and for c-C_3D, we accounted for 51 energy levels connected by 205 radiative transitions.
Results. Our results show that the $3_{31} \rightarrow 3_{30}$ transition of c-C_3H and c-C_3D may be found in absorption against the cosmic microwave background (CMB). Furthermore, we found population inversion for the $1_{10} \rightarrow 1_{11}$ transition. These findings may be useful in identifying these molecules in other cosmic objects, as well as for the determination of physical parameters in these objects.

Key words. ISM: molecules – molecular data

1. Introduction

Cyclopropynylidyne, c-C_3H, was the second hydrocarbon ring molecule found in interstellar space (after c-C_3H_2). It was first detected by Yamamoto et al. (1987) in TMC-1, who observed the $2_{12} \rightarrow 1_{11}$ transition at 91.5 GHz in emission. Later, Mangum & Wootten (1990) observed the transition $1_{10} \rightarrow 1_{11}$ at 14.8 GHz in emission in 12 additional galactic objects. The linear isotopomer l-C_3H has also been identified in TMC-1 and IRC +10216 (Thaddeus et al. 1985). The most probable production mechanism of C_3H and C_3H_2 in dark clouds is a common dissociation reaction of the $C_3H_3^+$ ion (Adams & Smith 1987). Although c-C_3H is 0.8 eV less stable than l-C_3H, the column density of c-C_3H is found almost comparable to that of l-C_3H in TMC-1.

We have performed NLTE radiative transfer calculations for c-C_3H and c-C_3D. Our results indicate that the $3_{31} \rightarrow 3_{30}$ transition will show up in absorption against the CMB over a wide range of physical parameters. In addition, we found population inversion in a certain parameter range for the $1_{10} \rightarrow 1_{11}$ transition. These findings may be useful for identifying these molecules and for determination of the physical conditions within the objects where they are found. In this investigation we did not account for fine and hyperfine splittings of the levels.

2. Basic formulation

The c-C_3H and c-C_3D both are a-type asymmetric top molecules with equal electric dipole moment $\mu = 2.4$ Debye. Rotational levels in an asymmetric top molecule are specified as J_{k_a,k_c}, where J is the rotational quantum number and k_a and k_c the projections of J on the axis of symmetry in case of prolate and oblate symmetric tops, respectively. In an a-type asymmetric top molecule, rotational radiative transitions are governed by the selection rules:

$$\begin{aligned} J: &\quad \Delta J = 0 \pm 1 \\ k_a, k_c: &\quad \text{even, odd} \longleftrightarrow \text{even, even} \\ : &\quad \text{odd, even} \longleftrightarrow \text{odd, odd.} \end{aligned}$$

Owing to the nuclear symmetry in c-C_3H and c-C_3D, the rotational levels with even value of k_a are missing in their spectra. In the present investigation we accounted for the rotational levels up to 106 cm^{-1} for c-C_3H (Fig. 1, Table 1) and up to 94 cm^{-1} for c-C_3D (Table 2).

In our investigation, NLTE occupation numbers are calculated in an on-the-spot approximation based on an escape probability method. For this we used a VLG (large velocity gradient) code (Goldreich & Kwan 1974) in the form as described by Rausch et al. (1996), where the external radiation field is assumed to be the CMB only. In this approximation, the escape probabilities depend on the local occupation numbers only. Inserting these into the rate equations, the latter become nonlinear. For c-C_3H, a set of 51 nonlinear rate equations involving 207 radiative transitions and for c-C_3D, a set of 51 nonlinear rate equations involving 205 radiative transitions are solved by iteration for the given values of the hydrogen density n_{H_2} and of the parameter $\gamma \equiv n_{\rm mol}/(\mathrm{d}v_r/\mathrm{d}r)$, $n_{\rm mol}$ being the density of the molecule and $(\mathrm{d}v_r/\mathrm{d}r)$ the velocity gradient in the object. The input data required in the present investigation are the radiative transition probabilities (Einstein A-coefficients) and the collisional rate coefficients.

⋆ Tables 1–3 and Figs. 4, 5 are only available in electronic form at http://www.aanda.org

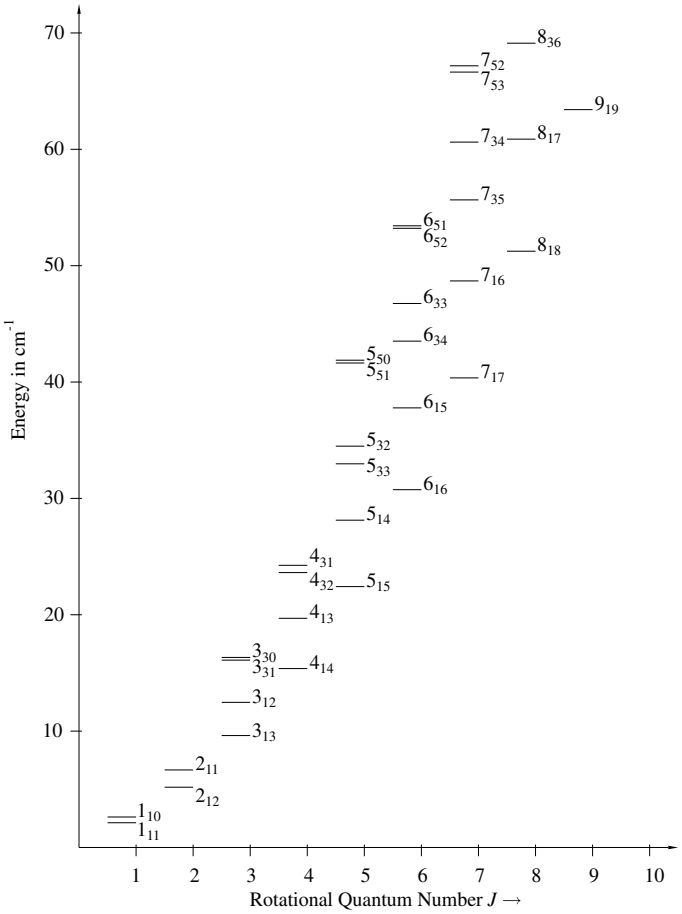

Fig. 1. Energy level diagram for c-C_3H.

2.1. Einstein A-coefficients

The energy levels and Einstein A-coefficients of radiatively allowed transitions are calculated as described by Chandra et al. (1984) and Chandra & Rashmi (1998). The required rotational and distortional constants are taken from Yamamoto & Saito (1994). The numerical values of the energy levels and the Einstein A-coefficients are given in Tables 1–3.

2.2. Collisional rate coefficients

Since rate coefficients for collisions with H_2 molecules are not available in the literature, we assumed for the downward transitions $J'k'_ak'_c \rightarrow Jk_ak_c$ at a kinetic temperature T_k:

$$C(J'k'_ak'_c \rightarrow Jk_ak_c) = 1 \times 10^{-11}\,(2J+1)\sqrt{\frac{T_k}{30}}. \quad (1)$$

The upward collisional rate coefficients were determined using the detailed balancing equations.

3. Anomalous absorption and population inversion

The observation of a spectral line in absorption against the CMB is a phenomenon as unusual as the occurrence of population inversion (maser emission) as discussed e.g. by ter Haar & Pelling (1974). Both phenomena are a sign of extreme deviation from LTE. They do not show up if one models the molecules as two level systems, i.e. for any theoretical explanation, three or more energy levels have to be accounted for.

The intensity, I_ν, of a line formed in an interstellar cloud, with homogeneous excitation conditions, is given by

$$I_\nu - I_{\nu,\mathrm{bg}} = (S_\nu - I_{\nu,\mathrm{bg}})\,(1 - \mathrm{e}^{-\tau_\nu}) \quad (2)$$

where $I_{\nu,\mathrm{bg}}$ is the intensity of the continuum against which the line is observed, τ_ν being the optical depth of the line, and S_ν the source function. Expressing the intensity I_ν in terms of the brightness temperature T_B, and the source function S_ν in terms of the excitation temperature T_ex, Eq. (2) may also be written in the form (Rayleigh Jeans approximation):

$$T_\mathrm{B} - T_{\nu,\mathrm{bg}} = (T_\mathrm{ex} - T_{\nu,\mathrm{bg}})\,(1 - \mathrm{e}^{-\tau_\nu}). \quad (3)$$

Whether a given line appears in absorption or in emission, depends in general on the physical conditions within the cloud where it is formed and on the background against which it is observed. In the case of anomalous absorption, i.e. if we have $0 < T_\mathrm{ex} < T_\mathrm{CMB}$, where T_CMB is 2.73 K, however, the line will appear in absorption against any background, even against the CMB. Similarly, in case we have an occupation inversion, in which case T_ex and τ_ν both are negative, the line will appear in emission against any background.

4. Results and discussion

In order to include a large number of cosmic objects where c-C_3H and c-C_3D may be found, numerical calculations are carried out for wide ranges of physical parameters. The molecular hydrogen density n_{H_2} has been varied over the range from 10^3 cm^{-3} to 10^7 cm^{-3} and calculations are performed for kinetic temperatures from 10 K to 70 K and for two values of γ, 10^{-5} cm^{-3}(km/s)$^{-1}$pc and 10^{-6}cm^{-3}(km/s)$^{-1}$pc. In the calculations, the molecular hydrogen density n_{H_2}, the kinetic temperature T_k and γ are free parameters. As we have used scaled values of collisional rates, our results are qualitative in nature.

4.1. The c-C_3H radical

Figures 2–4 show the results of our numerical computations for three particular lines of the c-C_3H radical, the $3_{31} \rightarrow 3_{30}$ transition at 3.4 GHz, the $1_{10} \rightarrow 1_{11}$ transition at 14.8 GHz, and the $2_{12} \rightarrow 1_{11}$ transition at 91.5 GHz.

The figures give the relative brightness temperatures – i.e. the quantity $(T_\mathrm{B} - T_{\nu,\mathrm{bg}})/T_{\nu,\mathrm{bg}}$ – for two different backgrounds, the first being the CMB and the second a non-thermal source corresponding to Cas A. The latter background was determined by taking the brightness temperature at 14.5 GHz from the map of Batrla et al. (1983) at the position where Yamamoto et al. searched for the 91.5 GHz line and then scaling it to the frequencies of our lines according to the frequency dependence as determined by Baars et al. (1977) and adding the CMB. In addition, the figures show the optical depth, and in case of the 3.4 GHz line the excitation temperature. All these quantities are shown as functions of n_{H_2} for given values of T_k and γ.

We found a number of lines of c-C_3H to occur in absorption against the CMB, the transition $3_{31} \rightarrow 3_{30}$ at 3.4 GHz (Fig. 2) being the strongest one.

We note in particular, that for a given kinetic temperature, the excitation temperature T_ex first decreases with increasing values of n_{H_2}, then goes through a wide minimum and finally increases again. This general behavior can be understood by qualitative arguments: since in the limit $n_{\mathrm{H}_2} \rightarrow 0$ the radiative transition rates dominate over the collisional rates, we have $T_\mathrm{ex} \rightarrow T_\mathrm{CMB}$.

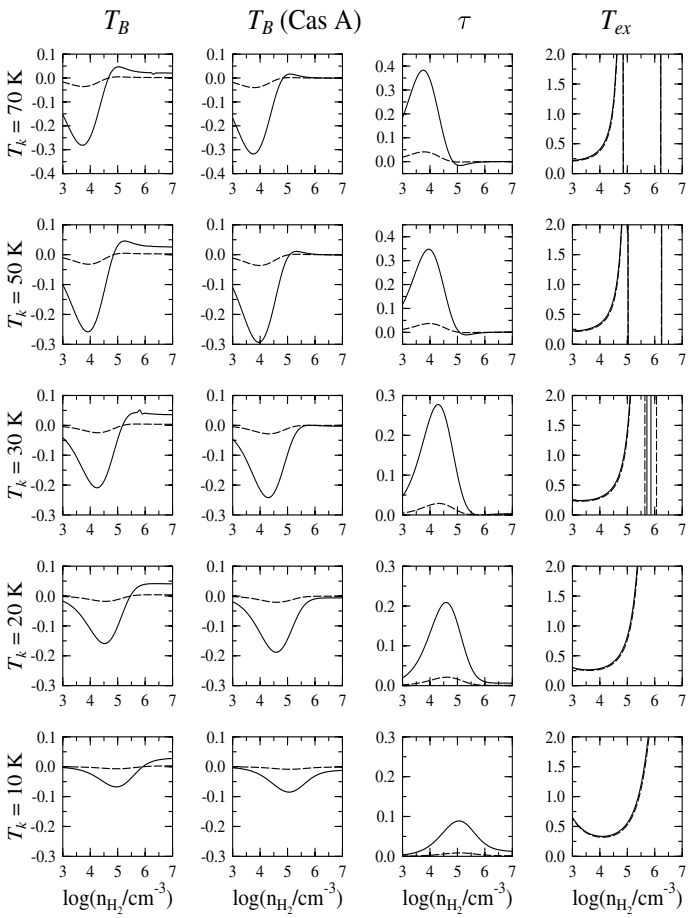

Fig. 2. Results for the transition $3_{31} \rightarrow 3_{30}$ of c-C_3H. T_B: relative brightness temperature with respect to the CMB, T_B (Cas A): with respect to a non-thermal source like Cas A (see text), τ: optical depth and T_{ex}: excitation temperature. All quantities are given as function of hydrogen density n_{H_2} for given values of kinetic temperatures T_k (10, 20, 30, 50, 70 K). Solid line is for $\gamma = 10^{-5}$ cm^{-3} (km/s)$^{-1}$ pc and dashed line for $\gamma = 10^{-6}$ cm^{-3} (km/s)$^{-1}$ pc.

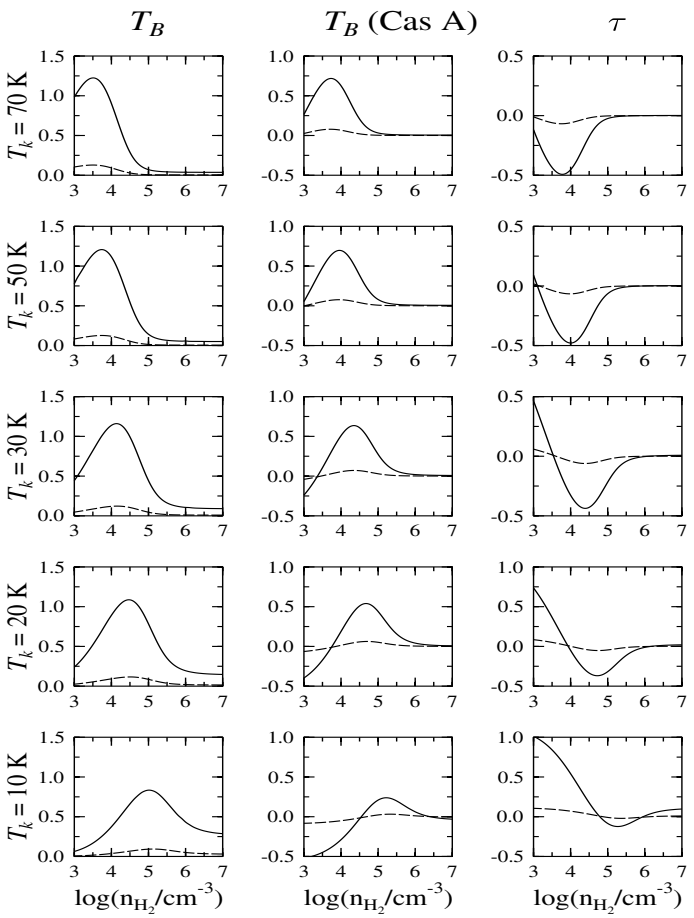

Fig. 3. Same as Fig. 2 but for the transition $1_{10} \rightarrow 1_{11}$ of c-C_3H.

In the other limit, $n_{H_2} \rightarrow \infty$, the collisional transition rates dominate and we have $T_{ex} \rightarrow T_k$. In the range in between the two limits, the excitation of most of the levels is dominated by the collisions, while in the optically thin limit the deexcitation rate for most of the levels is determined by spontaneous emission. In this range, one finds as a crude estimate for a line for which the energy difference between the upper and the lower level is small compared to kT and small as compared to the excitation energy of both levels – conditions satisfied for the $3_{31} \rightarrow 3_{30}$ transition of c-C_3H – that the ratio of the occupation numbers of the upper and the lower level is roughly given by the inverse of the radiative life times of the levels. For the $3_{31} \rightarrow 3_{30}$ transition, this value is 0.53 (see Table 1). Since T_{ex} is defined through the ratio of the occupation numbers, this explains why the minimum of T_{ex} as function of n_{H_2} is so wide. The variation of T_{ex} with the kinetic temperature T_k is essentially a consequence of the variation of the upward collision rates with T_k. (The excitation energies of 3_{31} and 3_{30} levels are of the order of 20 K, see Fig. 1) The collision rates increase with T_k. The most important effect of this is that the above discussed limits are shifted to lower densities. It is noteworthy that in the density range for which we have $T_{ex} < T_{CMB}$, T_{ex} varies considerably less with T_k than T_B and τ. This is due to the fact that T_{ex} depends only on the *ratio* of the occupation numbers, while τ depends on the *difference*.

From Fig. 2 we also see that at higher temperatures ($T_k \geq 30$ K) there is a small range of densities in which we have population inversion.

The curves for T_{ex} calculated for the two values of γ hardly differ from each other. This indicates that optical thickness effects are unimportant in this parameter range.

From our numerical results, we also find population inversion for several transitions, the most important one being the transition $1_{10} \rightarrow 1_{11}$ (Fig. 3). The inversion indicated in Fig. 3 by negative values of τ, is a consequence of the interplay between collisional and radiative transitions. Collisions provide in our model the basic excitation. Therefore at low densities, the inversion increases with increasing density, goes through a maximum (minimum of τ) and then decreases again. In this context we note that the minimum of τ occurs approximately when the collisional and the radiative lifetime of the upper level become equal. The strong dependence on the kinetic temperature shows that the higher lying energy levels are involved. The higher levels are excited by collisions and then are deexcited mostly due to radiative transitions. In this context we note, that the radiative lifetime of the 1_{10} level is larger than that of all other levels by more than one order of magnitude (see Tables 1 and 2).

Figure 4 shows the results for the $2_{12} \rightarrow 1_{11}$ transition at 91.5 GHz, which was observed by Yamamoto et al. (1987) in TMC-1 and searched for in the direction of Cas A. At this high frequency, the non-thermal background is very low and therefore has only little effect on the appearance of the line.

4.2. The c-C_3D radical

The results we obtained for the c-C_3D radical are qualitatively very similar to those found for c-C_3H. In particular, we found for the $3_{31} \rightarrow 3_{30}$ transition at 0.9 GHz anomalous absorption, and for the $1_{10} \rightarrow 1_{11}$ transition at 10.8 GHz population inversion over a wide range of parameters. We shall not go into a detailed discussion, but just refer to Fig. 5 showing the results for the $3_{31} \rightarrow 3_{30}$ transition of c-C_3D.

5. Conclusions

Our numerical results show that in a range of physical parameters typical for interstellar molecular clouds, strong deviations from LTE of the relative occupation numbers of the molecules c-C_3H and c-C_3D are to be expected. For certain transitions these may imply anomalous absorption or population inversion. Therefore, it is difficult to derive the total column density of a given molecule by observing just one line. For a quantitative estimate of the column density and other physical parameters one should measure several lines, if possible. In this context the observation of anomalous absorption may be of particular use, since this phenomenon is restricted to a certain range of densities. If observations are made against a non-thermal background source, the $1_{10} \rightarrow 1_{11}$ transition may be found in emission or absorption, depending on the physical parameters within the cloud in which the line is formed.

Acknowledgements. Financial supports from the Department of Science & Technology, New Delhi and the Indian Space Research Organisation, Bangalore in the form of research projects are thankfully acknowledged. Suresh Chandra is grateful to Prof. Dr. W. H. Kegel and Prof. Dr. E. Sedlmayr for their kind invitation and hospitality under scientific exchange programme between the Indian National Science Academy (INSA), New Delhi, India and the Deutsche Forschungsgemeinschaft (DFG), Bonn, Germany.

References

Adams, N. G., & Smith, D. 1987, ApJ, 317, L25
Baars, J. W. M., Genzel, R., Pauliny-Thoth, I. I. K., & Witzel, A. 1977, A&A, 61, 99
Batrla, W., Wilson, T. L., & Martin-Pintado, J. 1983, A&A, 119 139
Chandra, S., & Rashmi 1998, A&AS, 131, 137
Chandra, S. Varshalovich, D. A., & Kegel, W. H 1984, A&AS, 55, 51
Goldreich, P., & Kwan, J. 1974, ApJ, 189, 144
Mangum, J. G., & Wootten, A. 1990, A&A, 239, 319
Rausch, E., Kegel, W. H., Tsuji, T., & Piehler, G. 1996, A&A, 315, 533
Thaddeus, P., Gottlieb, C. A., Hjalmarson, A., et al. 1985a, ApJ, 294, L49
ter Haar, D., & Pelling, M. A. 1974, Rep. Prog. Phys., 37, 481
Yamamoto, S., & Saito, S. 1994, J. Chem. Phys., 101, 5484
Yamamoto, S., Saito, S., Ohishi, M., et al. 1987, ApJ, 322, L55

Online Material

Table 1. Energy (in cm^{-1}) and radiative lifetime of rotational levels for c-C_3H.

c-C_3H					
Level	Energy	Radiative lifetime	Level	Energy	Radiative lifetime
1_{11}	2.126	–	6_{51}	53.378	1.366×10^3
1_{10}	2.620	9.154×10^6	7_{35}	55.653	7.619×10^2
2_{12}	5.180	6.473×10^4	7_{34}	60.619	4.920×10^2
2_{11}	6.664	2.716×10^4	8_{17}	60.874	7.136×10^2
3_{13}	9.620	1.698×10^4	9_{19}	63.410	6.772×10^2
3_{12}	12.472	7.708×10^3	7_{53}	66.637	6.905×10^2
4_{14}	15.376	7.202×10^3	7_{52}	67.177	5.496×10^2
3_{31}	16.174	4.354×10^4	8_{36}	69.120	5.407×10^2
3_{30}	16.289	2.341×10^4	9_{18}	74.336	5.187×10^2
4_{13}	19.696	3.930×10^3	8_{35}	75.712	3.860×10^2
5_{15}	22.421	3.762×10^3	$10_{1,10}$	76.856	4.969×10^2
4_{32}	23.625	4.990×10^3	7_{71}	79.382	4.208×10^3
4_{31}	24.249	3.139×10^3	7_{70}	79.383	4.184×10^3
5_{14}	28.128	2.389×10^3	8_{54}	81.887	4.069×10^2
6_{16}	30.748	2.215×10^3	8_{53}	83.447	2.937×10^2
5_{33}	32.792	2.059×10^3	9_{37}	83.878	4.015×10^2
5_{32}	34.490	1.247×10^3	10_{19}	89.075	3.890×10^2
6_{15}	37.780	1.525×10^3	$11_{1,11}$	91.582	3.753×10^2
7_{17}	40.356	1.413×10^3	9_{36}	91.921	3.078×10^2
5_{51}	41.864	9.225×10^3	8_{72}	94.551	7.785×10^2
5_{50}	41.876	8.606×10^3	8_{71}	94.564	7.669×10^2
6_{34}	43.515	1.162×10^3	9_{55}	98.849	2.774×10^2
6_{33}	46.751	7.036×10^2	10_{38}	99.916	3.073×10^2
7_{16}	48.690	1.020×10^3	9_{54}	102.033	1.915×10^2
8_{18}	51.243	9.565×10^2	$11_{1,10}$	105.094	2.993×10^2
6_{52}	53.262	1.535×10^3			

Table 2. Energy (in cm^{-1}) and radiative lifetime of rotational levels for c-C_3D.

c-C_3D					
Level	Energy	Radiative lifetime	Level	Energy	Radiative lifetime
1_{11}	2.055	–	6_{52}	50.330	3.149×10^3
1_{10}	2.416	2.345×10^7	6_{51}	50.341	3.094×10^3
2_{12}	4.695	1.002×10^5	7_{34}	52.136	7.462×10^2
2_{11}	5.779	4.762×10^4	8_{17}	54.024	9.862×10^2
3_{13}	8.586	2.491×10^4	9_{19}	56.415	9.523×10^2
3_{12}	10.724	1.204×10^4	8_{36}	61.196	7.746×10^2
4_{14}	13.678	1.024×10^4	7_{53}	61.292	1.350×10^3
3_{31}	15.684	9.167×10^4	7_{52}	61.354	1.291×10^3
3_{30}	15.715	6.745×10^4	8_{35}	65.525	5.118×10^2
4_{13}	17.096	5.301×10^3	9_{18}	66.018	7.221×10^2
5_{15}	19.936	5.290×10^3	$10_{1,10}$	68.385	6.994×10^2
4_{32}	21.876	9.020×10^3	8_{54}	73.889	7.498×10^2
4_{31}	22.072	7.098×10^3	8_{53}	74.128	6.798×10^2
5_{14}	24.694	3.075×10^3	9_{37}	74.279	5.643×10^2
6_{16}	27.344	3.107×10^3	7_{71}	78.161	1.042×10^4
5_{33}	29.596	3.478×10^3	7_{70}	78.161	1.042×10^4
5_{32}	30.257	2.513×10^3	10_{19}	79.144	5.436×10^2
6_{15}	33.385	2.017×10^3	9_{36}	80.234	3.884×10^2
7_{17}	35.894	1.983×10^3	$11_{1,11}$	81.493	5.287×10^2
6_{34}	38.778	1.833×10^3	9_{55}	88.099	4.763×10^2
6_{33}	40.314	1.243×10^3	10_{38}	88.540	4.289×10^2
5_{51}	40.995	2.248×10^4	9_{54}	88.796	4.004×10^2
5_{50}	40.996	2.224×10^4	8_{72}	90.575	1.649×10^3
7_{16}	43.153	1.388×10^3	8_{71}	90.575	1.648×10^3
8_{18}	45.585	1.344×10^3	$11_{1,10}$	93.406	4.192×10^2
7_{35}	49.339	1.134×10^3			

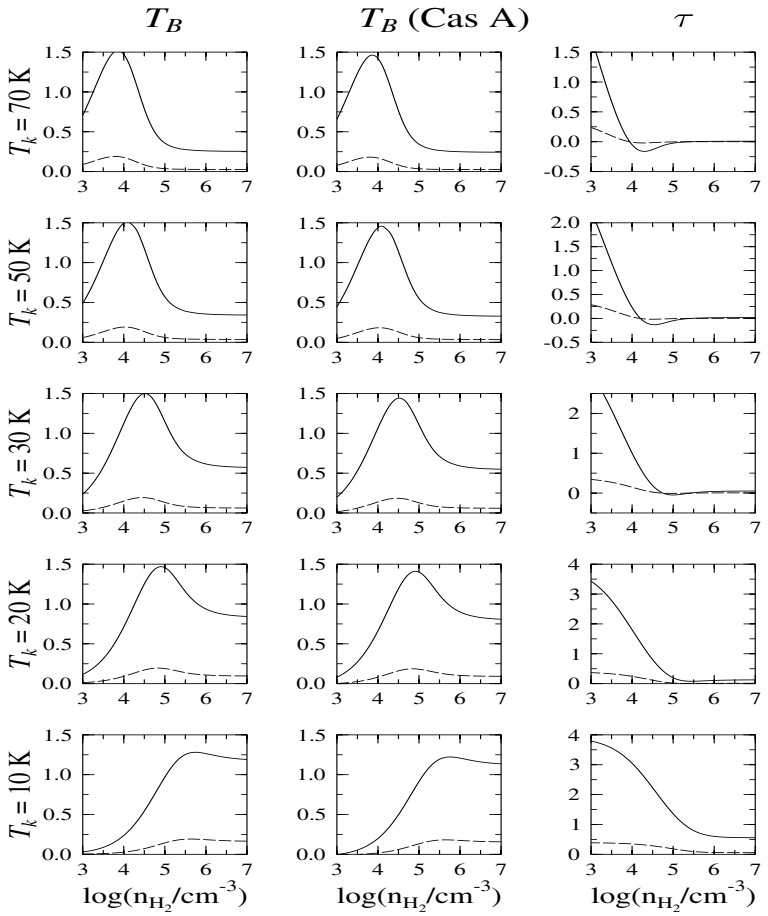

Fig. 4. Same as Fig. 2 but for the transition $2_{12} \rightarrow 1_{11}$ of c-C_3H.

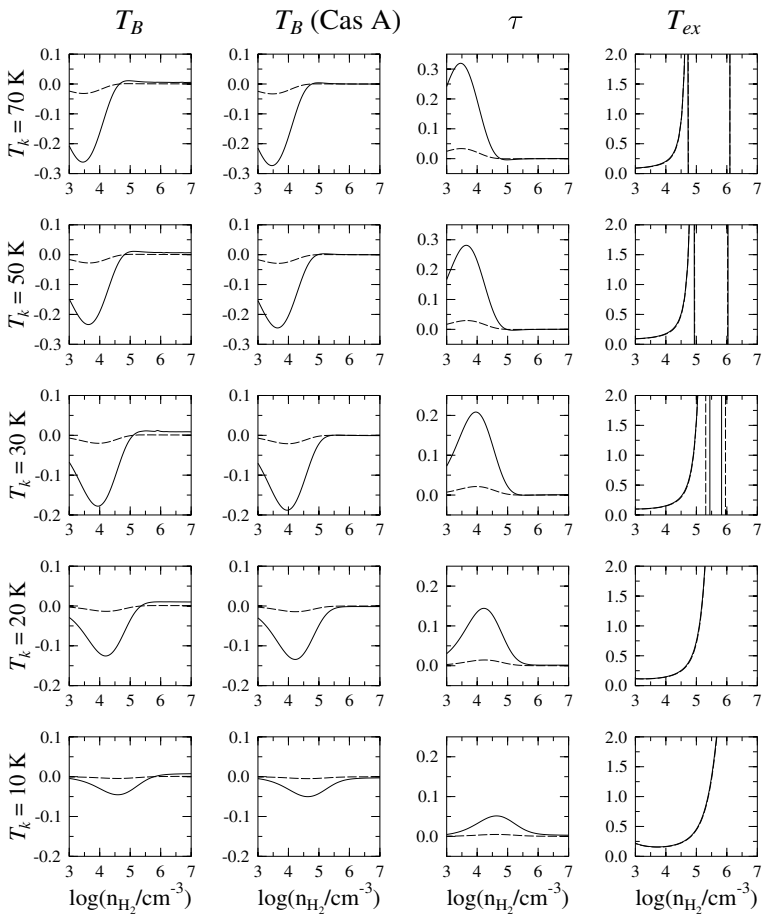

Fig. 5. Same as Fig. 2 but for the transition $3_{31} \rightarrow 3_{30}$ of c-C_3D.

Table 3: Einstein coefficients for C_3H and C_3D

For C_3H		
1(1, 0) → 1(1, 1) 1.092×10^{-7}	2(1, 2) → 1(1, 1) 1.545×10^{-5}	2(1, 1) → 1(1, 0) 3.584×10^{-5}
2(1, 1) → 2(1, 2) 9.831×10^{-7}	3(1, 3) → 2(1, 2) 5.889×10^{-5}	3(1, 2) → 2(1, 1) 1.257×10^{-4}
3(1, 2) → 3(1, 3) 4.002×10^{-6}	4(1, 4) → 3(1, 3) 1.389×10^{-4}	3(3, 1) → 2(1, 2) 1.995×10^{-5}
3(3, 1) → 3(1, 2) 3.014×10^{-6}	3(3, 1) → 4(1, 4) 2.508×10^{-10}	3(3, 0) → 2(1, 1) 4.142×10^{-5}
3(3, 0) → 3(1, 3) 1.305×10^{-6}	3(3, 0) → 3(3, 1) 1.908×10^{-9}	4(1, 3) → 3(1, 2) 2.435×10^{-4}
4(1, 3) → 4(1, 4) 1.061×10^{-5}	4(1, 3) → 3(3, 0) 3.081×10^{-7}	5(1, 5) → 4(1, 4) 2.658×10^{-4}
4(3, 2) → 3(1, 3) 4.337×10^{-5}	4(3, 2) → 3(3, 1) 1.487×10^{-4}	4(3, 2) → 4(1, 3) 8.287×10^{-6}
4(3, 2) → 5(1, 5) 8.248×10^{-10}	4(3, 1) → 3(1, 2) 1.299×10^{-4}	4(3, 1) → 4(1, 4) 1.576×10^{-6}
4(3, 1) → 3(3, 0) 1.869×10^{-4}	4(3, 1) → 4(3, 2) 1.543×10^{-7}	5(1, 4) → 4(1, 3) 3.977×10^{-4}
5(1, 4) → 5(1, 5) 2.052×10^{-5}	5(1, 4) → 4(3, 1) 3.912×10^{-7}	6(1, 6) → 5(1, 5) 4.515×10^{-4}
5(3, 3) → 4(1, 4) 6.497×10^{-5}	5(3, 3) → 4(3, 2) 4.038×10^{-4}	5(3, 3) → 5(1, 4) 1.684×10^{-5}
5(3, 3) → 6(1, 6) 2.854×10^{-9}	5(3, 2) → 4(1, 3) 1.927×10^{-4}	5(3, 2) → 5(1, 5) 1.218×10^{-6}
5(3, 2) → 4(3, 1) 6.062×10^{-4}	5(3, 2) → 5(3, 3) 1.710×10^{-6}	6(1, 5) → 5(1, 4) 6.226×10^{-4}
6(1, 5) → 6(1, 6) 3.318×10^{-5}	6(1, 5) → 5(3, 2) 9.906×10^{-8}	7(1, 7) → 6(1, 6) 7.076×10^{-4}
5(5, 1) → 4(1, 4) 4.361×10^{-7}	5(5, 1) → 4(3, 2) 1.024×10^{-4}	5(5, 1) → 5(1, 4) 9.009×10^{-7}
5(5, 1) → 6(1, 6) 8.847×10^{-10}	5(5, 1) → 5(3, 2) 4.653×10^{-6}	5(5, 0) → 4(1, 3) 6.517×10^{-6}
5(5, 0) → 5(1, 5) 5.816×10^{-8}	5(5, 0) → 4(3, 1) 1.045×10^{-4}	5(5, 0) → 5(3, 3) 5.144×10^{-6}
5(5, 0) → 6(1, 5) 2.562×10^{-9}	5(5, 0) → 5(5, 1) 2.567×10^{-12}	6(3, 4) → 5(1, 5) 8.492×10^{-5}
6(3, 4) → 5(3, 3) 7.452×10^{-4}	6(3, 4) → 6(1, 5) 3.042×10^{-5}	6(3, 4) → 7(1, 7) 7.213×10^{-9}
6(3, 4) → 5(5, 1) 3.216×10^{-9}	6(3, 3) → 5(1, 4) 2.179×10^{-4}	6(3, 3) → 6(1, 6) 9.835×10^{-7}
6(3, 3) → 5(3, 2) 1.194×10^{-3}	6(3, 3) → 5(5, 0) 2.716×10^{-7}	6(3, 3) → 6(3, 4) 7.956×10^{-6}
7(1, 6) → 6(1, 5) 9.319×10^{-4}	7(1, 6) → 7(1, 7) 4.864×10^{-5}	7(1, 6) → 6(3, 3) 8.744×10^{-9}
8(1, 8) → 7(1, 7) 1.046×10^{-3}	6(5, 2) → 5(1, 5) 9.224×10^{-7}	6(5, 2) → 5(3, 3) 2.426×10^{-4}
6(5, 2) → 6(1, 5) 2.250×10^{-6}	6(5, 2) → 7(1, 7) 1.720×10^{-9}	6(5, 2) → 5(5, 1) 3.939×10^{-4}
6(5, 2) → 6(3, 3) 1.187×10^{-5}	6(5, 1) → 5(1, 4) 1.914×10^{-5}	6(5, 1) → 6(1, 6) 1.042×10^{-7}
6(5, 1) → 5(3, 2) 2.965×10^{-4}	6(5, 1) → 5(5, 0) 4.052×10^{-4}	6(5, 1) → 6(3, 4) 1.122×10^{-5}
6(5, 1) → 7(1, 6) 5.325×10^{-9}	6(5, 1) → 6(5, 2) 1.486×10^{-9}	7(3, 5) → 6(1, 6) 1.046×10^{-4}
7(3, 5) → 6(3, 4) 1.158×10^{-3}	7(3, 5) → 7(1, 6) 5.006×10^{-5}	7(3, 5) → 8(1, 8) 1.393×10^{-8}
7(3, 5) → 6(5, 2) 1.920×10^{-8}	7(3, 4) → 6(1, 5) 2.583×10^{-4}	7(3, 4) → 7(1, 7) 9.389×10^{-7}
7(3, 4) → 6(3, 3) 1.746×10^{-3}	7(3, 4) → 6(5, 1) 3.482×10^{-6}	7(3, 4) → 7(3, 5) 2.375×10^{-5}
8(1, 7) → 7(1, 6) 1.334×10^{-3}	8(1, 7) → 8(1, 8) 6.700×10^{-5}	8(1, 7) → 7(3, 4) 1.112×10^{-11}
9(1, 9) → 8(1, 8) 1.477×10^{-3}	7(5, 3) → 6(1, 6) 1.093×10^{-6}	7(5, 3) → 6(3, 4) 3.978×10^{-4}
7(5, 3) → 7(1, 6) 3.192×10^{-6}	7(5, 3) → 8(1, 8) 2.079×10^{-9}	7(5, 3) → 6(5, 2) 1.024×10^{-3}
7(5, 3) → 7(3, 4) 2.205×10^{-5}	7(5, 2) → 6(1, 5) 2.142×10^{-5}	7(5, 2) → 7(1, 7) 8.708×10^{-8}
7(5, 2) → 6(3, 3) 6.463×10^{-4}	7(5, 2) → 6(5, 1) 1.138×10^{-3}	7(5, 2) → 7(3, 5) 1.388×10^{-5}
7(5, 2) → 8(1, 7) 7.628×10^{-9}	7(5, 2) → 7(5, 3) 9.674×10^{-8}	8(3, 6) → 7(1, 7) 1.244×10^{-4}
8(3, 6) → 7(3, 5) 1.649×10^{-3}	8(3, 6) → 8(1, 7) 7.592×10^{-5}	8(3, 6) → 9(1, 9) 2.244×10^{-8}
8(3, 6) → 7(5, 3) 2.314×10^{-8}	9(1, 8) → 8(1, 7) 1.840×10^{-3}	9(1, 8) → 9(1, 9) 8.831×10^{-5}
8(3, 5) → 7(1, 6) 3.172×10^{-4}	8(3, 5) → 8(1, 8) 9.671×10^{-7}	8(3, 5) → 7(3, 4) 2.214×10^{-3}
8(3, 5) → 7(5, 2) 7.796×10^{-6}	8(3, 5) → 8(3, 6) 5.098×10^{-5}	8(3, 5) → 9(1, 8) 1.332×10^{-9}
10(1,10) → 9(1, 9) 2.012×10^{-3}	7(7, 1) → 6(1, 6) 3.640×10^{-9}	7(7, 1) → 6(3, 4) 1.910×10^{-6}
7(7, 1) → 7(1, 6) 2.136×10^{-8}	7(7, 1) → 8(1, 8) 1.698×10^{-11}	7(7, 1) → 6(5, 2) 2.268×10^{-4}
7(7, 1) → 7(3, 4) 9.831×10^{-7}	7(7, 1) → 7(5, 2) 7.964×10^{-6}	7(7, 1) → 8(3, 6) 2.473×10^{-9}
7(7, 0) → 6(1, 5) 1.342×10^{-7}	7(7, 0) → 7(1, 7) 5.939×10^{-10}	7(7, 0) → 6(3, 3) 4.792×10^{-6}
7(7, 0) → 6(5, 1) 2.251×10^{-4}	7(7, 0) → 7(3, 5) 2.700×10^{-7}	7(7, 0) → 8(1, 7) 4.275×10^{-10}
7(7, 0) → 7(5, 3) 8.660×10^{-6}	7(7, 0) → 8(3, 5) 1.522×10^{-9}	8(5, 4) → 7(1, 7) 1.023×10^{-6}
8(5, 4) → 7(3, 5) 5.404×10^{-4}	8(5, 4) → 8(1, 7) 3.616×10^{-6}	8(5, 4) → 9(1, 9) 2.083×10^{-9}
8(5, 4) → 7(5, 3) 1.876×10^{-3}	8(5, 4) → 8(3, 5) 3.686×10^{-5}	8(5, 4) → 7(7, 1) 6.608×10^{-9}
8(5, 3) → 7(1, 6) 1.384×10^{-5}	8(5, 3) → 8(1, 8) 4.594×10^{-8}	8(5, 3) → 7(3, 4) 9.875×10^{-4}
8(5, 3) → 7(5, 2) 2.390×10^{-3}	8(5, 3) → 8(3, 6) 1.210×10^{-5}	8(5, 3) → 9(1, 8) 8.049×10^{-9}
8(5, 3) → 7(7, 0) 3.512×10^{-8}	8(5, 3) → 8(5, 4) 1.448×10^{-6}	9(3, 7) → 8(1, 8) 1.443×10^{-4}
9(3, 7) → 8(3, 6) 2.238×10^{-3}	9(3, 7) → 9(1, 8) 1.078×10^{-4}	9(3, 7) → 10(1,10) 3.216×10^{-8}
9(3, 7) → 8(5, 4) 9.861×10^{-9}	10(1, 9) → 9(1, 8) 2.458×10^{-3}	10(1, 9) → 10(1,10) 1.126×10^{-4}
11(1,11) → 10(1,10) 2.664×10^{-3}	9(3, 6) → 8(1, 7) 3.788×10^{-4}	9(3, 6) → 9(1, 9) 9.924×10^{-7}
9(3, 6) → 8(3, 5) 2.778×10^{-3}	9(3, 6) → 8(5, 3) 4.698×10^{-6}	9(3, 6) → 9(3, 7) 8.670×10^{-5}
9(3, 6) → 10(1, 9) 8.612×10^{-9}	8(7, 2) → 7(1, 7) 8.928×10^{-9}	8(7, 2) → 7(3, 5) 6.688×10^{-6}
8(7, 2) → 8(1, 7) 5.863×10^{-8}	8(7, 2) → 9(1, 9) 3.926×10^{-11}	8(7, 2) → 7(5, 3) 5.264×10^{-4}
8(7, 2) → 8(3, 5) 4.679×10^{-6}	8(7, 2) → 7(7, 1) 7.284×10^{-4}	8(7, 2) → 8(5, 3) 1.826×10^{-5}
8(7, 2) → 9(3, 7) 6.677×10^{-9}	8(7, 1) → 7(1, 6) 3.958×10^{-7}	8(7, 1) → 8(1, 8) 1.393×10^{-9}
8(7, 1) → 7(3, 4) 3.236×10^{-5}	8(7, 1) → 7(5, 2) 5.185×10^{-4}	8(7, 1) → 8(3, 6) 8.468×10^{-7}
8(7, 1) → 9(1, 8) 1.097×10^{-9}	8(7, 1) → 7(7, 0) 7.301×10^{-4}	8(7, 1) → 8(5, 4) 2.168×10^{-5}
8(7, 1) → 9(3, 6) 1.950×10^{-9}	8(7, 1) → 8(7, 2) 2.457×10^{-12}	9(5, 5) → 8(1, 8) 8.843×10^{-7}
9(5, 5) → 8(3, 6) 6.649×10^{-4}	9(5, 5) → 9(1, 8) 3.769×10^{-6}	9(5, 5) → 10(1,10) 1.954×10^{-9}
9(5, 5) → 8(5, 4) 2.876×10^{-3}	9(5, 5) → 9(3, 6) 5.973×10^{-5}	9(5, 5) → 8(7, 2) 1.028×10^{-7}
10(3, 8) → 9(1, 9) 1.643×10^{-4}	10(3, 8) → 9(3, 7) 2.945×10^{-3}	10(3, 8) → 10(1, 9) 1.456×10^{-4}

Table 3: Continued.

10(3, 8)	→ 11(1,11)	4.269×10^{-8}	10(3, 8)	→ 9(5, 5)	1.147×10^{-9}	9(5, 4)	→ 8(1, 7)	7.853×10^{-6}
9(5, 4)	→ 9(1, 9)	2.218×10^{-8}	9(5, 4)	→ 8(3, 5)	1.091×10^{-3}	9(5, 4)	→ 8(5, 3)	4.103×10^{-3}
9(5, 4)	→ 9(3, 7)	9.715×10^{-6}	9(5, 4)	→ 10(1, 9)	7.308×10^{-9}	9(5, 4)	→ 8(7, 1)	1.025×10^{-6}
9(5, 4)	→ 9(5, 5)	8.376×10^{-6}	11(1,10)	→ 10(1, 9)	3.201×10^{-3}	11(1,10)	→ 11(1,11)	1.398×10^{-4}
				For C_3D				
1(1, 0)	→ 1(1, 1)	4.264×10^{-8}	2(1, 2)	→ 1(1, 1)	9.976×10^{-6}	2(1, 1)	→ 1(1, 0)	2.062×10^{-5}
2(1, 1)	→ 2(1, 2)	3.838×10^{-7}	3(1, 3)	→ 2(1, 2)	4.014×10^{-5}	3(1, 2)	→ 2(1, 1)	8.153×10^{-5}
3(1, 2)	→ 3(1, 3)	1.552×10^{-6}	4(1, 4)	→ 3(1, 3)	9.761×10^{-5}	3(3, 1)	→ 2(1, 2)	8.966×10^{-6}
3(3, 1)	→ 3(1, 2)	1.938×10^{-6}	3(3, 1)	→ 4(1, 4)	4.254×10^{-9}	3(3, 0)	→ 2(1, 1)	1.354×10^{-5}
3(3, 0)	→ 3(1, 3)	1.281×10^{-6}	3(3, 0)	→ 3(3, 1)	3.744×10^{-11}	4(1, 3)	→ 3(1, 2)	1.843×10^{-4}
4(1, 3)	→ 4(1, 4)	4.359×10^{-6}	4(1, 3)	→ 3(3, 0)	9.545×10^{-9}	5(1, 5)	→ 4(1, 4)	1.890×10^{-4}
4(3, 2)	→ 3(1, 3)	2.148×10^{-5}	4(3, 2)	→ 3(3, 1)	8.422×10^{-5}	4(3, 2)	→ 4(1, 3)	5.159×10^{-6}
4(3, 2)	→ 5(1, 5)	5.430×10^{-9}	4(3, 1)	→ 3(1, 2)	4.713×10^{-5}	4(3, 1)	→ 4(1, 4)	2.374×10^{-6}
4(3, 1)	→ 3(3, 0)	9.138×10^{-5}	4(3, 1)	→ 4(3, 2)	5.569×10^{-9}	5(1, 4)	→ 4(1, 3)	3.156×10^{-4}
5(1, 4)	→ 5(1, 5)	9.474×10^{-6}	5(1, 4)	→ 4(3, 1)	1.528×10^{-7}	6(1, 6)	→ 5(1, 5)	3.219×10^{-4}
5(3, 3)	→ 4(1, 4)	3.520×10^{-5}	5(3, 3)	→ 4(3, 2)	2.426×10^{-4}	5(3, 3)	→ 5(1, 4)	9.727×10^{-6}
5(3, 3)	→ 6(1, 6)	7.749×10^{-9}	5(3, 2)	→ 4(1, 3)	1.017×10^{-4}	5(3, 2)	→ 5(1, 5)	2.611×10^{-6}
5(3, 2)	→ 4(3, 1)	2.935×10^{-4}	5(3, 2)	→ 5(3, 3)	1.266×10^{-7}	6(1, 5)	→ 5(1, 4)	4.788×10^{-4}
6(1, 5)	→ 6(1, 6)	1.673×10^{-5}	6(1, 5)	→ 5(3, 2)	2.448×10^{-7}	7(1, 7)	→ 6(1, 6)	5.042×10^{-4}
6(3, 4)	→ 5(1, 5)	4.835×10^{-5}	6(3, 4)	→ 5(3, 3)	4.810×10^{-4}	6(3, 4)	→ 6(1, 5)	1.613×10^{-5}
6(3, 4)	→ 7(1, 7)	1.275×10^{-8}	6(3, 3)	→ 5(1, 4)	1.465×10^{-4}	6(3, 3)	→ 6(1, 6)	2.258×10^{-6}
6(3, 3)	→ 5(3, 2)	6.547×10^{-4}	6(3, 3)	→ 6(3, 4)	9.829×10^{-7}	5(5, 1)	→ 4(1, 4)	1.829×10^{-7}
5(5, 1)	→ 4(3, 2)	4.033×10^{-5}	5(5, 1)	→ 5(1, 4)	4.054×10^{-7}	5(5, 1)	→ 6(1, 6)	1.796×10^{-9}
5(5, 1)	→ 5(3, 2)	3.557×10^{-6}	5(5, 1)	→ 6(3, 4)	4.170×10^{-9}	5(5, 0)	→ 4(1, 3)	1.142×10^{-6}
5(5, 0)	→ 5(1, 5)	4.823×10^{-8}	5(5, 0)	→ 4(3, 1)	3.990×10^{-5}	5(5, 0)	→ 5(3, 3)	3.869×10^{-6}
5(5, 0)	→ 6(1, 5)	8.863×10^{-9}	5(5, 0)	→ 6(3, 3)	1.641×10^{-10}	7(1, 6)	→ 6(1, 5)	6.946×10^{-4}
7(1, 6)	→ 7(1, 7)	2.567×10^{-5}	7(1, 6)	→ 6(3, 3)	1.067×10^{-7}	8(1, 8)	→ 7(1, 7)	7.442×10^{-4}
7(3, 5)	→ 6(1, 6)	6.070×10^{-5}	7(3, 5)	→ 6(3, 4)	7.958×10^{-4}	7(3, 5)	→ 7(1, 6)	2.525×10^{-5}
7(3, 5)	→ 8(1, 8)	2.118×10^{-8}	6(5, 2)	→ 5(1, 5)	5.917×10^{-7}	6(5, 2)	→ 5(3, 3)	9.650×10^{-5}
6(5, 2)	→ 6(1, 5)	1.630×10^{-6}	6(5, 2)	→ 7(1, 7)	4.714×10^{-9}	6(5, 2)	→ 6(3, 3)	8.558×10^{-6}
6(5, 2)	→ 5(5, 1)	2.103×10^{-4}	6(5, 2)	→ 7(3, 5)	1.035×10^{-9}	6(5, 1)	→ 5(1, 4)	6.365×10^{-6}
6(5, 1)	→ 6(1, 6)	1.413×10^{-7}	6(5, 1)	→ 5(3, 2)	9.601×10^{-5}	6(5, 1)	→ 6(3, 4)	9.686×10^{-6}
6(5, 1)	→ 5(5, 0)	2.109×10^{-4}	6(5, 1)	→ 7(1, 6)	2.208×10^{-8}	6(5, 1)	→ 6(5, 2)	1.402×10^{-12}
7(3, 4)	→ 6(1, 5)	1.670×10^{-4}	7(3, 4)	→ 7(1, 7)	1.886×10^{-6}	7(3, 4)	→ 6(3, 3)	1.167×10^{-3}
7(3, 4)	→ 7(3, 5)	4.062×10^{-6}	7(3, 4)	→ 6(5, 1)	1.055×10^{-8}	8(1, 7)	→ 7(1, 6)	9.778×10^{-4}
8(1, 7)	→ 8(1, 8)	3.616×10^{-5}	8(1, 7)	→ 7(3, 4)	1.634×10^{-8}	9(1, 9)	→ 8(1, 8)	1.050×10^{-3}
8(3, 6)	→ 7(1, 7)	7.266×10^{-5}	8(3, 6)	→ 7(3, 5)	1.180×10^{-3}	8(3, 6)	→ 8(1, 7)	3.782×10^{-5}
8(3, 6)	→ 9(1, 9)	3.312×10^{-8}	7(5, 3)	→ 6(1, 6)	1.051×10^{-6}	7(5, 3)	→ 6(3, 4)	1.701×10^{-4}
7(5, 3)	→ 7(1, 6)	3.332×10^{-6}	7(5, 3)	→ 8(1, 8)	7.366×10^{-9}	7(5, 3)	→ 6(5, 2)	5.515×10^{-4}
7(5, 3)	→ 7(3, 4)	1.466×10^{-5}	7(5, 3)	→ 8(3, 6)	1.521×10^{-12}	7(5, 2)	→ 6(1, 5)	1.588×10^{-5}
7(5, 2)	→ 7(1, 7)	2.273×10^{-7}	7(5, 2)	→ 6(3, 3)	1.831×10^{-4}	7(5, 2)	→ 7(3, 5)	1.609×10^{-5}
7(5, 2)	→ 6(5, 1)	5.593×10^{-4}	7(5, 2)	→ 8(1, 7)	3.362×10^{-8}	7(5, 2)	→ 7(5, 3)	1.764×10^{-10}
8(3, 5)	→ 7(1, 6)	1.834×10^{-4}	8(3, 5)	→ 8(1, 8)	1.700×10^{-6}	8(3, 5)	→ 7(3, 4)	1.757×10^{-3}
8(3, 5)	→ 8(3, 6)	1.171×10^{-5}	8(3, 5)	→ 7(5, 2)	3.631×10^{-7}	9(1, 8)	→ 8(1, 7)	1.337×10^{-3}
9(1, 8)	→ 9(1, 9)	4.827×10^{-5}	9(1, 8)	→ 8(3, 5)	1.661×10^{-10}	10(1,10)	→ 9(1, 9)	1.430×10^{-3}
8(5, 4)	→ 7(1, 7)	1.358×10^{-6}	8(5, 4)	→ 7(3, 5)	2.568×10^{-4}	8(5, 4)	→ 8(1, 7)	4.865×10^{-6}
8(5, 4)	→ 9(1, 9)	8.978×10^{-9}	8(5, 4)	→ 7(5, 3)	1.048×10^{-3}	8(5, 4)	→ 8(3, 5)	2.229×10^{-5}
8(5, 3)	→ 7(1, 6)	2.353×10^{-5}	8(5, 3)	→ 8(1, 8)	2.532×10^{-7}	8(5, 3)	→ 7(3, 4)	3.313×10^{-4}
8(5, 3)	→ 8(3, 6)	2.125×10^{-5}	8(5, 3)	→ 7(5, 2)	1.095×10^{-3}	8(5, 3)	→ 9(1, 8)	4.186×10^{-8}
8(5, 3)	→ 8(5, 4)	7.366×10^{-9}	9(3, 7)	→ 8(1, 8)	8.458×10^{-5}	9(3, 7)	→ 8(3, 6)	1.633×10^{-3}
9(3, 7)	→ 9(1, 8)	5.417×10^{-5}	9(3, 7)	→ 10(1,10)	4.809×10^{-8}	9(3, 7)	→ 8(5, 4)	1.112×10^{-10}
7(7, 1)	→ 6(1, 6)	1.521×10^{-9}	7(7, 1)	→ 6(3, 4)	3.832×10^{-7}	7(7, 1)	→ 7(1, 6)	1.033×10^{-8}
7(7, 1)	→ 8(1, 8)	2.834×10^{-11}	7(7, 1)	→ 6(5, 2)	8.913×10^{-5}	7(7, 1)	→ 7(3, 4)	1.494×10^{-7}
7(7, 1)	→ 8(3, 6)	3.646×10^{-9}	7(7, 1)	→ 7(5, 2)	6.289×10^{-6}	7(7, 1)	→ 8(5, 4)	1.153×10^{-8}
7(7, 0)	→ 6(1, 5)	2.965×10^{-8}	7(7, 0)	→ 7(1, 7)	4.738×10^{-10}	7(7, 0)	→ 6(3, 3)	4.595×10^{-7}
7(7, 0)	→ 7(3, 5)	1.019×10^{-7}	7(7, 0)	→ 6(5, 1)	8.905×10^{-5}	7(7, 0)	→ 8(1, 7)	5.469×10^{-10}
7(7, 0)	→ 7(5, 3)	6.345×10^{-6}	7(7, 0)	→ 8(3, 5)	5.131×10^{-9}	7(7, 0)	→ 8(5, 3)	9.803×10^{-9}
10(1, 9)	→ 9(1, 8)	1.778×10^{-3}	10(1, 9)	→ 10(1,10)	6.203×10^{-5}	9(3, 6)	→ 8(1, 7)	2.104×10^{-4}
9(3, 6)	→ 9(1, 9)	1.678×10^{-6}	9(3, 6)	→ 8(3, 5)	2.334×10^{-3}	9(3, 6)	→ 8(5, 3)	2.196×10^{-6}
9(3, 6)	→ 9(3, 7)	2.658×10^{-5}	9(3, 6)	→ 10(1, 9)	1.320×10^{-9}	11(1,11)	→ 10(1,10)	1.892×10^{-3}
9(5, 5)	→ 8(1, 8)	1.450×10^{-6}	9(5, 5)	→ 8(3, 6)	3.469×10^{-4}	9(5, 5)	→ 9(1, 8)	5.905×10^{-6}
9(5, 5)	→ 10(1,10)	9.524×10^{-9}	9(5, 5)	→ 8(5, 4)	1.713×10^{-3}	9(5, 5)	→ 9(3, 6)	3.200×10^{-5}
10(3, 8)	→ 9(1, 9)	9.661×10^{-5}	10(3, 8)	→ 9(3, 7)	2.161×10^{-3}	10(3, 8)	→ 10(1, 9)	7.431×10^{-5}
10(3, 8)	→ 11(1,11)	6.532×10^{-8}	10(3, 8)	→ 9(5, 5)	1.606×10^{-10}	9(5, 4)	→ 8(1, 7)	2.363×10^{-5}
9(5, 4)	→ 9(1, 9)	2.085×10^{-7}	9(5, 4)	→ 8(3, 5)	5.526×10^{-4}	9(5, 4)	→ 8(5, 3)	1.898×10^{-3}

Table 3: Continued.

9(5, 4)	→	9(3, 7)	2.306×10^{-5}	9(5, 4)	→	10(1, 9)	4.519×10^{-8}	9(5, 4)	→	9(5, 5)	1.298×10^{-7}
8(7, 2)	→	7(1, 7)	6.134×10^{-9}	8(7, 2)	→	7(3, 5)	1.786×10^{-6}	8(7, 2)	→	8(1, 7)	4.599×10^{-8}
8(7, 2)	→	9(1, 9)	1.017×10^{-10}	8(7, 2)	→	7(5, 3)	2.005×10^{-4}	8(7, 2)	→	8(3, 5)	9.681×10^{-7}
8(7, 2)	→	8(5, 3)	1.605×10^{-5}	8(7, 2)	→	9(3, 7)	1.368×10^{-8}	8(7, 2)	→	7(7, 1)	3.870×10^{-4}
8(7, 2)	→	9(5, 5)	7.633×10^{-9}	8(7, 1)	→	7(1, 6)	1.536×10^{-7}	8(7, 1)	→	8(1, 8)	1.808×10^{-9}
8(7, 1)	→	7(3, 4)	2.880×10^{-6}	8(7, 1)	→	8(3, 6)	4.585×10^{-7}	8(7, 1)	→	7(5, 2)	1.996×10^{-4}
8(7, 1)	→	9(1, 8)	2.118×10^{-9}	8(7, 1)	→	8(5, 4)	1.659×10^{-5}	8(7, 1)	→	7(7, 0)	3.870×10^{-4}
8(7, 1)	→	9(3, 6)	2.109×10^{-8}	8(7, 1)	→	9(5, 4)	2.957×10^{-9}	11(1,10)	→	10(1, 9)	2.308×10^{-3}
11(1,10)	→	11(1,11)	7.748×10^{-5}								